Al-Nahrain Journal of Science
ANJS, Vol. 29 (1), March, 2026, pp. 31 – 41

Syntheses, Characterization, DFT and Molecular Docking of N-(4-chlorophenyl)-1-(4-nitrophenyl) methanimine, (4-chlorophenyl)-1-(4-methoxyphenyl) methanimine and its derivatives

Asya A. Tawfiq[1], Omar J. Mahdi[2], Ahmed H. Hattab[3]

[1] Department of Chemistry, College of Education for Women, Tikrit University, Tikrit, Iraq.
[2] Department of Chemistry, Education College for Pure Science, University of Anbar, Anbar, Iraq
[3] Department of Chemistry, College of Science, University of Kirkuk, Kirkuk, Iraq.

Article's Information

Received: 21.07.2025
Accepted: 14.12.2025
Published: 15.03.2026

Keywords:
Imines,
Schiff bases,
Molecular Docking,
DFT.

Abstract

The synthesis of numerous chemical compounds relies on imines as a key building ingredient. Several Schiff bases were generated via the acid-catalyzed condensation of aromatic aldehyde derivatives with aniline derivatives. FT-IR, ^{1}HNMR, spectra allowed to identify the products. The ORCA software package was used to obtain the outcome of the Density Functional Theory (DFT) and to comprehend how para substituting impacts the electronic structure of the synthesized compounds. Finally, docking simulation was performed using the Autodock application. At the binding site, the prepared compounds were docked with the 3FYV enzyme.

http://doi.org/10.22401/ANJS.29.1.04

*Corresponding author: omar.j.m@uoanbar.edu.iq

1. Introduction

Schiff base compounds are the most significant family of chemicals containing an imide group (HC=N-), also called an imine group. [1]. The Schiff base domain has undergone significant expansion owing to the plethora of prospective product designs that can be generated from the examined active compounds containing (C=O) and (-NH2) as functional groups. [2]. Various Schiff bases have demonstrated pharmacological applications, where several previous studies examined their effectiveness as antis, such as bacterial [3], tumors [4], fungal [5], oxidant [6], enzyme-inhibitory [7], cancer [8], inflammatory [9], hypertensive [10], glycation [11], anti-HIV [12], tuberculosis [13], seizure [14], and antineurotoxic activities [15]. Chemical interactions, reactivity, and selectivity can be described by computing the eigenvalues. The energy levels between them can be characterized by these physical characteristics. [15] A frontier-molecular orbital (FMO) is the energy level between a molecular orbital with the least amount of occupancy (LUMO) and one with the most HOMO. These levels are used to describe the spectroscopic behavior, reactivity, and kinetic studies [16]. The current study focused on maintaining the same para-position of the aromatic ring while varying the type of substituted group. Our study clarifies the difference of the type of the substituted group on the electronic properties using the Orca program. In addition, the current study demonstrated that molecular docking analysis provided a conclusive confirmation of the interaction between the synthetic chemicals and the enzymes, suggesting that Schiff base molecules may possess antibacterial properties.

2. Materials and Methods

Benzaldehyde (P-NO_2, P-OCH_3) and (P-Cl, P-CH_3) aniline. The solvents were provided by Scharlau Company, while the chemicals were sourced from Sigma-Aldrich Chemical Co., Infrared spectra, were recorded using a Bruker-Tensor 27 spectrometer and ^{1}H-NMR spectra were obtained with Bruker-400 MHz spectrometer.

3. Experimental

3.1. Procedure

The formation of compounds A1-A4 was illustrated in Figure 1.

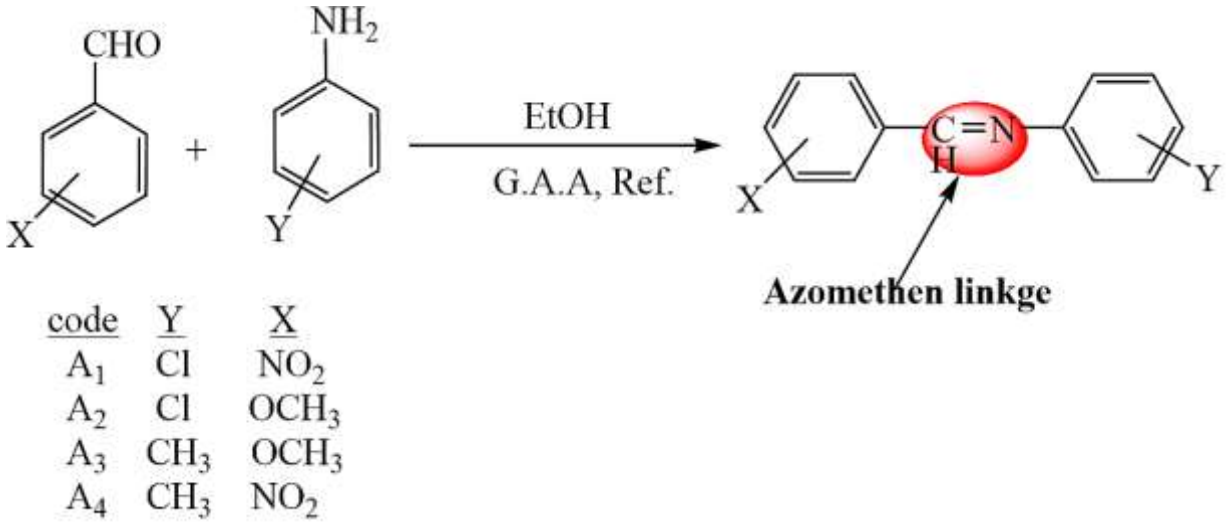

code	Y	X
A_1	Cl	NO_2
A_2	Cl	OCH_3
A_3	CH_3	OCH_3
A_4	CH_3	NO_2

Figure 1. Route for synthetic of compounds

3.2. Prepare of N-(4-chlorophenyl)-1-(4-nitrophenyl) methanimine A1 and other derivatives [17]

A 100 mL round-bottom, two-necked flask was used to combine a solution of (p-NO_2) benzaldehyde (0.01 mol) in absolute ethanol (10 mL) with a few drops of glacial acetic acid. This solution was then mixed with p-chloroaniline (0.01 mol.) dissolved in absolute ethanol (15 mL). After refluxing for 4 hours, the resulting precipitate was filtered and recrystallized from the same solvent. Further derivatives were synthesized using the same procedure.

Table 1 Characterization of the produced compounds

	Properties					
Code	Color	yield	M.P°C	IR spectra v (cm-1)	R*f* Eluent (9:1) (benz:MeOH)	1H-NMR (δ, ppm)
A1	Yellow	83%	194-196	(C-H arom.)3099 (C=N)1624(C=C) 1597, 1487), (C-N) 1008C-NO2 sy. 1371C-NO2 asy.1340	0.81	8H arom, m, 7.36- 8.40 1H-CH=N-, s 8.91
A2	White	74%	142-144	(C-H arom.) 3018 (C=N) 1619(C=C) 1567, 1477(C-N)1090C-H alip. 2962	0.75	3H methoxy., s 3.818H arom , m7.06- 7.891H -CH=N- ,s 8.39
A3	White	71%	153-155	(C-H arom.)3077, (C=N)1621, (C=C) 1595,1504(C-N)1022C-H alip. 2971	0.79	3H methyl., s, 2.098H arom , m7.49- 7.741H-CH=N-, s 8.33
A4	Yellow	79%	136-138	(C-H arom.)3078 (C=N) 1625 (C=C) 1596, 1514 (C-N)1005C-NO2 sy. 1376C-NO2 asy.1339	0.73	3H methyl., s, 2.108H arom , m8.22- 8.411H-CH=N- , s 8.92

4. Characterization

Table 1 provides a summary of the Schiff base derivatives' characteristics.

5. Computational Details

The Avogadro program (version 1.2.0n) graphical user interface was used to build the input structures of the synthesized compounds A1–A4 [18–20]. The ORCA software package (version 4.2.1) was employed to perform quantum chemical calculations using Kohn–Sham DFT. For each atom, the def2-SVP basis set [21] was applied for vibrational frequency calculations and geometry optimizations.

Molecular docking studies of the prepared samples were carried out and analyzed using ChimeraX 1.9, Discovery Studio, and AutoDock 4.2.

6. Results and Discussion

6.1. FT-IR Spectra

In the range of 1619-1625 cm^{-1}, imines typically show a robust -CH=N- stretching vibration. The skeletal structure of the imine compounds is supported by the presence of a -CH=N- stretching band. Aromatic C–H stretching vibrations were observed in the wide range of 2319-3052 cm^{-1}. The compounds were validated by the observed C-H stretching frequencies, which included imine, aliphatic, and aromatic groups. Table 1 displays the infrared spectral values of compounds A1-A4. [22]

6.2. ^{1}H-NMR spectra

DMSOd^6 solvent was used to record the 1H-NMR spectra. Position, multiplicities, and integral values dictated the assignment and establishment of signals in the ^{1}H-NMR spectra. Aromatic proton signals usually appeared in the higher frequency range of 7.00-8.50 ppm due to the magnetic anisotropic effect. Imine compound derivatives' ^{1}H-NMR spectra show signals in the 7.06-8.41 ppm range, which are consistent with eight protons integral caused by aromatic protons. ^{1}H (-CH=N-) is characterized by a singular signal at 8.33–8.92 ppm. The ^{1}H-NMR spectra of Compound A are presented in Figure 1. (S1) [23]

6.3. Computational Study

The ORCA software package (DFT), with the B3LYP functional and the def2-SVP basis set, was used to calculate the electronic characteristics of compounds A1–A4. These calculations included HOMO, LUMO, and many electronic properties. Reactive compounds have tiny Egap, whereas stable, unreactive molecules have wide Egap. Higher HOMO energies facilitate electron donation, while diminished LUMO energies enhance electron acceptance. Computational studies show that the A1-A4 molecule is more stable and has a higher LUMO energy level than other compounds synthesized by substituting halogen. For the compounds A1-A4, there is an energy difference between their HOMO and LUMO orbitals. To understand this more, table 2 contains the outcomes of the computations for the electronic properties, such as electrophilicity ω, absolute electronegativity μ, absolute hardness η, ionization potential I, and electron affinity A. [24]

$$A = -(E_{LUMO}) \qquad I = -(E_{HOMO}) \qquad \omega = \frac{\mu^2}{2\eta}$$

$$\mu = \frac{E_{LUMO} + E_{HOMO}}{2} \qquad \eta = \frac{E_{LUMO} - E_{HOMO}}{2}$$

Table 2. Electronic properties of compounds A1-A4

code	HOMO & LUMO and Property (a.u)									
	E_{HOMO}	E_{LUMO}	E_{gap}	I	A	χ	M	H	δ	Ω
A1	-6.44	-2.94	3.5	6.44	2.94	4.69	- 4.69	1.75	0.28	2.68
A2	-5.76	-1.65	4.11	5.76	1.65	3.70	- 3.70	2.05	0.24	4.35
A3	-5.58	-1.44	4.14	5.58	1.44	3.51	- 3.51	2.07	0.24	4.45
A4	-6.27	-2.79	3.57	6.27	2.79	4.53	- 4.53	1.74	0.28	2.64
μ= Chemical potential, η=Global hardness, δ= Global softness, I=Ionization energy, A=Electron affinity, χ= Electronegativity, ω= Global electrophilicity index										

Frontier molecular orbitals are classified as either the lowest unoccupied molecular orbitals (LUMO), which denote the ability to take electrons, or the highest occupied molecular orbitals (HOMO), which have the capacity to donate them. These orbitals are crucial in determining the chemical compound's stability. The table (2) shows the results of the DFT calculation of the HOMO and LUMO energy levels at the B3LYP/def2-SVP level of theory. When a molecule is electronically excited, an electron is promoted from the highest occupied molecular orbital (HOMO) to the lowest unoccupied molecular orbital (LUMO) . The complex interactions among molecules and their chemical stability are dictated by the energy difference between them.[25-26]. Fig. 2 illustrates the diagram of the Egap, and Fig 3 the distribution of electronic densities for Schiff bases' HOMO and LUMO states.

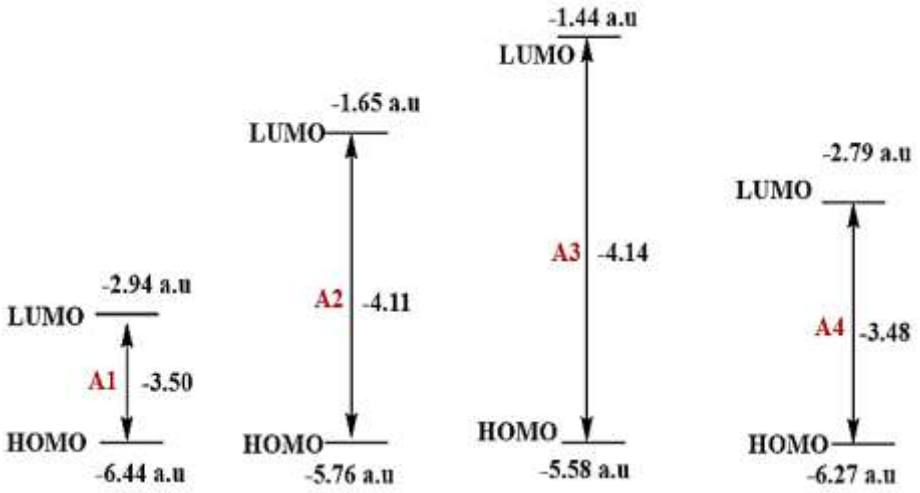

Figure 2. displays the diagram of the HOMO-LUMO energy value

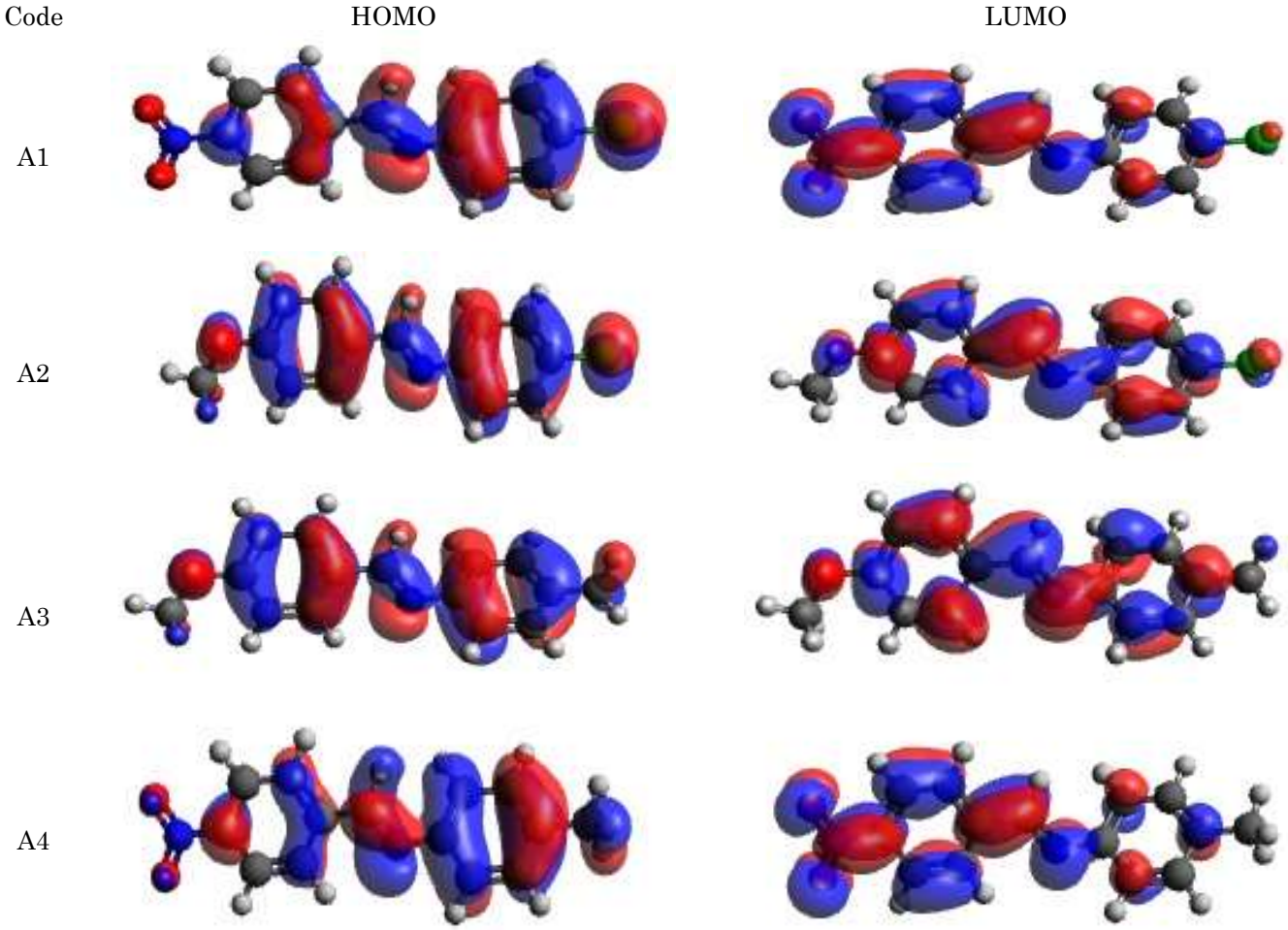

Figure 3. The distribution of electronic densities for Schiff bases' HOMO and LUMO states is depicted

6.4..Atomic Charges

Atomic charges affect the electronic structure, polarizability, dipole moment, and other characteristics of molecular systems. When applying quantum chemical calculations to molecular systems, Mulliken atomic charge is a crucial factor. Mulliken atomic charges for compounds A1–A4 are computed and listed in Table 3. We note from the values in Table 3 that the C21 carries the highest positive charge, which is 0.1779, 0.2305, 0.2295 and 0.1772 which may be due to the attachment of the NO_2 atom. Also, the nitrogen atom N10 carries the highest negative charge. As a result, the carbon atoms associated with nitrogen are electron acceptors, and their ability to receive electrons can be arranged as follows A4>A1>A3>A2 This is consistent with the type of substituent on the ring. When the substituent group is NO_2, it works to withdraw electrons, dissipating the positive charge. Therefore, the two compounds A4 and A1 have the lowest value 0.1772 and 0.1779. Moreover, these results are consistent with the results of Table 2, where we note that the energy gap values for the two compounds A4 and A1 have the lowest energy gap, which means that they are the most effective, confirming the validity of the results. [27-28].

Table 3. Mulliken atomic charges of compounds A1-A4

A1		A2		A3		A4	
Atoms	Charges	Atoms	Charges	Atoms	Charges	Atoms	Charges
1 C	0.0266	1 C	0.0233	1 C	-0.0137	1 C	-0.0198
2 Cl	-0.0932	2 Cl	-0.1065	2 C	0.0625	2 C	0.0851
3 H	-0.0131	3 H	-0.0193	3 H	-0.0299	3 H	-0.0286
4 C	0.0264	4 C	0.0246	4 C	-0.0121	4 C	-0.0177
5 C	-0.0246	5 C	-0.0282	5 C	-0.0228	5 C	-0.0121
6 H	-0.0102	6 H	-0.0173	6 H	-0.0274	6 H	-0.0269
7 C	0.0112	7 C	0.0043	7 C	0.0112	7 C	0.0223
8 C	0.0958	8 C	0.1009	8 C	0.0933	8 C	0.0821
9 H	-0.0181	9 H	-0.0233	9 H	-0.0317	9 H	-0.0285
10 N	-0.0708	10 N	-0.0862	10 N	-0.0848	10 N	-0.0696
11 C	0.0104	11 C	0.0089	11 C	0.0066	11 C	0.0075
12 H	-0.0186	12 H	-0.0273	12 H	-0.0297	12 H	-0.0214
13 H	-0.0166	13 H	-0.0236	13 H	-0.0331	13 H	-0.0267
14 C	0.0995	14 C	0.0784	14 C	0.0799	14 C	0.1011
15 C	-0.0172	15 C	-0.0157	15 C	-0.0164	15 C	-0.0180
16 H	-0.0090	16 H	-0.0199	16 H	-0.0213	16 H	-0.0107
17 C	0.0055	17 C	0.0051	17 C	0.0040	17 C	0.0042
18 C	-0.0059	18 C	-0.0093	18 C	-0.0100	18 C	-0.0066
19 H	0.0050	19 H	-0.0079	19 H	-0.0087	19 H	0.0040
20 C	-0.0026	20 C	-0.0686	20 C	-0.0692	20 C	-0.0032
21 C	0.1779	21 C	0.2305	21 C	0.2295	21 C	0.1772
22 H	0.0108	22 H	-0.0182	22 H	-0.0200	22 H	0.0091
23 H	0.0109	23 H	-0.0272	23 H	-0.0287	23 H	0.0092
24 N	0.2275	24 O	-0.3042	24 O	-0.3052	24 N	0.2275
25 O	-0.2354	25 C	0.1732	25 C	0.1741	25 O	-0.2372
26 O	-0.2365	26 H	0.0404	26 H	0.0391	26 O	-0.2385
		27 H	0.0238	27 H	0.0230	27 H	0.0063
		28 H	0.0263	28 H	0.0255	28 H	0.0288
				29 H	0.0036	29 H	0.0251
				30 H	0.0213		
				31 H	0.0203		

6.4. Molecular Docking of the prepared compounds

While the structure of Schiff base compounds was obtained from the synthesized compound, the crystal structures of the 3FYV enzyme were obtained from the Protein Database. The molecular docking simulation was carried out using bioinformatics tools

like the Autodock software to obtain understanding of the interaction that took place between the prepared compounds and the enzyme. Docking simulation was performed using the Autodock application. At the binding site, the prepared compounds were docked with the 3FYV enzyme. [24] The prepared compounds (A1–A4) were first built in Avogadro and saved in MOL2 format. Rotational bonds and torsions were then specified for each compound using MGLTools. Finally, each compound was converted into a PDBQT input file for docking studies The preparation of 3FYV models involved importing the relevant Protein Data bank files and using ChimeraX to remove non-standard residues such as NDP — nadph dihydro-nicotinamide-adenine-dinucleotidephosphate, XCF — 5-[[(2R)-2-cyclopropyl-7,8-dimethoxy-2H-chromen-5-yl] methyl]pyrimidine-2,4-diamine — and water were prepared as accepter. MGLTools was used to edit Kollman charges and add polar hydrogens, after which the structures were converted into PDBQT format following this setting, a gridbox then runs Autogrid and Autodock used Genetic Algorithem with the output Lamarckian and run with Autodock 4.2. To view and access the docking conformation, ChimeraX and Discovery Studio was used with the AutoDockTools analyse. Molecular docking results were analyzed using a variety of software, including ChimeraX, Discover studio, and Autodock 4.2. The primary purpose of the Discover studio program was to visualize the structures. All the protein's interaction residues as well as each compound were revealed using Autodock 4.2 software. Particularly for the screening of possible novel therapeutic molecules, molecular docking modeling is crucial. Our molecular docking modeling results of compounds with enzyme were contrasted. Analyze the prepared compounds potential as a novel inhibitor of the enzyme. The most promising enzyme exhibiting optimal interaction with A1-A4 was identified by the analysis of molecular docking findings involving the selected enzyme.

6.5. Creation of a hydrogen connection between the prepared chemicals and the enzyme

Hydrogen bond formation was the most important parameter for molecular docking study. The complex generated hydrogen bonds were seen using AutoDock 4.2 and ChimeraX. Discover Studio measured the distance and number of H-bonds created by the complexes and showed which protein parts formed hydrogen bonds with the chemical. The ideal hydrogen bonding distance [29] was roughly 1.5–2.6 Å. Additionally, the bond distance of the H-bond dictated the strength of the contact. A stronger contact between the protein and compound prepared is indicated by a shorter hydrogen bond length, which is indicative of a higher binding affinity of the complex. An H-bond is considered a weak contact that can be rapidly disrupted if the distance between the complex bindings exceeds 3.0 Å [30]. The outcomes have been identified via Discover Studio and ChimeraX, as illustrated in Table 4.

6.6. Results of molecular docking studies

We employed molecular docking to ascertain the proximity of target protein from bacterial species to all synthesized compounds (A1-A4). The examination of the 3FYV binding pockets produced ideal docking interaction scores and Table 4. Presents these scores, bond types, binding sites (A1-A4), active site amino acid residues, and the capacity of derivatives to occupy various locations. The Schiff base molecules may also have antibacterial properties, according to docking studies. The figures below display 3D and 2D representations of the interactions between the synthesized chemical derivatives and the amino acid residues located in the active sites of Escherichia coli [31].

Table 4. The obtained findings of binding energy and interaction residues.

Co.	Binding Energy kcal/mol	Interaction residues
A1	-7.77	HISx:30 and VALx:6(HB),VALx:31 and THRx:46(pi-Sigma), LEUx:5(Amide-pi), ALAx:7(pi-Alkyl
A2	-6.43	ALAx:7(HB),PHEx:92(CHB),VALx:6 and THRx:121(pi-DHB)
A3	-6.48	ESRx:49(HB),ASNx:18(CHB),VALx:6(Amidepi),LEUx:20,VALx:31,LEUx:5 and ALAx:7(pi-Alkly), VALx:31 and LEUx:5(Alkyl)
A4	-7.6	VALx:6,THRx:111 and HISx:30(HB),VALx:31(Pi Sigma) ,LEUx:5(Amide-Pi Stacked),ALAx:7(Pi-Alkyl)

When the binding energy of a complex is positive, it means that the binding is unstable; when it is negative, it means that the binding is stable as showed in Table 4. The results demonstrated that all complexes had negative binding energy values, which meant that the binding of the complex had been stabilized, and that the compounds that had been produced were appropriate for the 3FYV enzyme's specific binding site. In addition, as shown by molecular docking simulations, the binding energies of compounds A1, A2, A3, and A4 were (-7.77, -6.43, -6.48, -7.6 kcal/mol) respectively. The binding energy values of all compounds were Somewhat similar values, except for the 3FYV-A1 complex. [32-33] With the lowest binding energy value, the 3FYV-A1 combination stands out as the optimal ligand to form a complex with the 3FYV enzyme. This is because the strength of the binding contact between the protein and ligand complex is indicated by the binding affinity, which is larger when the binding energy value is lower. That A1 binds more strongly to the 3FYV binding site was thus validated by the research. The lowest binding affinity for 3FYV was shown by A2, which had the highest binding energy value of -6.43 kcal/mol. H-bond results are shown in Table 4 and A1 formed two H-bond with HIS30and VAL6 of the 3FYV enzyme, with a bond distance of 1.83Å and 2.50Å respectively as shown in Figure 4a. [34].

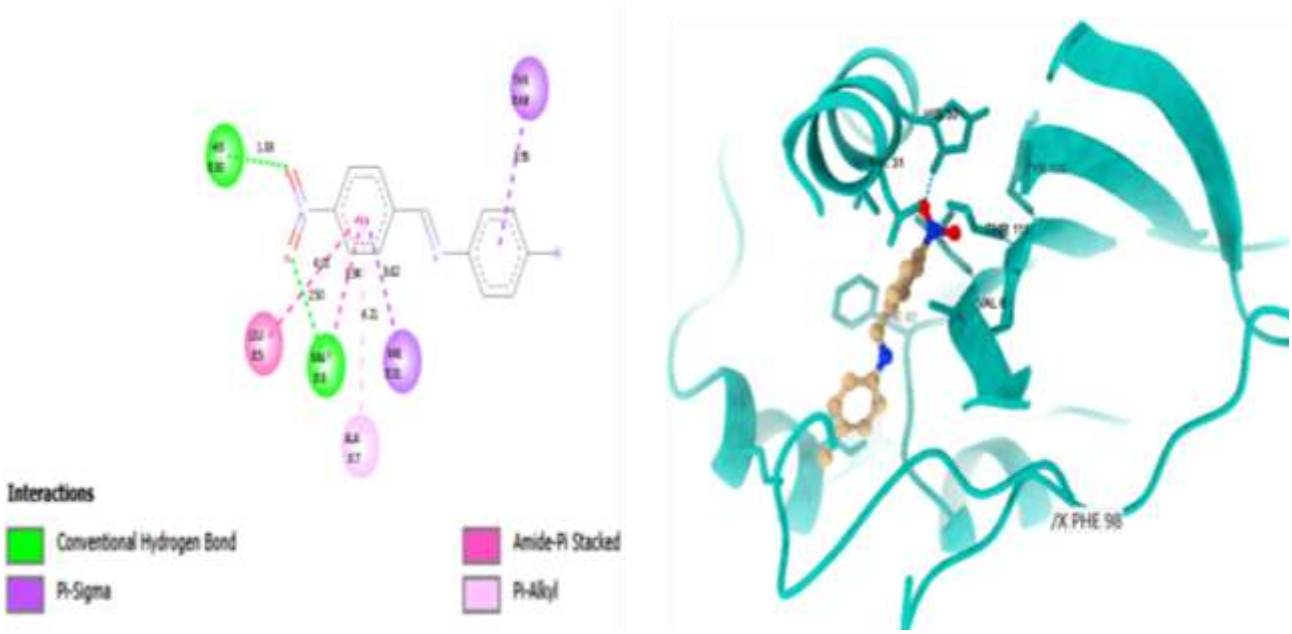

Figure4: a) Interaction between A1 and 3FYV, was illustrated using, Discover Studio diagram showing interaction tow hydrogen bonds (green dashed lines) with residues (HIS30, VAL6) at bond distances (1.83,2.50) Å respectively. Additionally, hydrophobic interaction observed were with (ALA7, LEU5, VAL31, THR46) which contribute to stabilization of the complex. (b) 3D interaction between A1 and 3FYV was illustrated using ChimeraX, shows the A1 was represented as sticks and balls (O as a red ball, N as a blue ball, and C as a yellow ball) bound with the active pocket of the 3FYV represented as a light sea green ribbon with one H-bond with residue (HIS30).

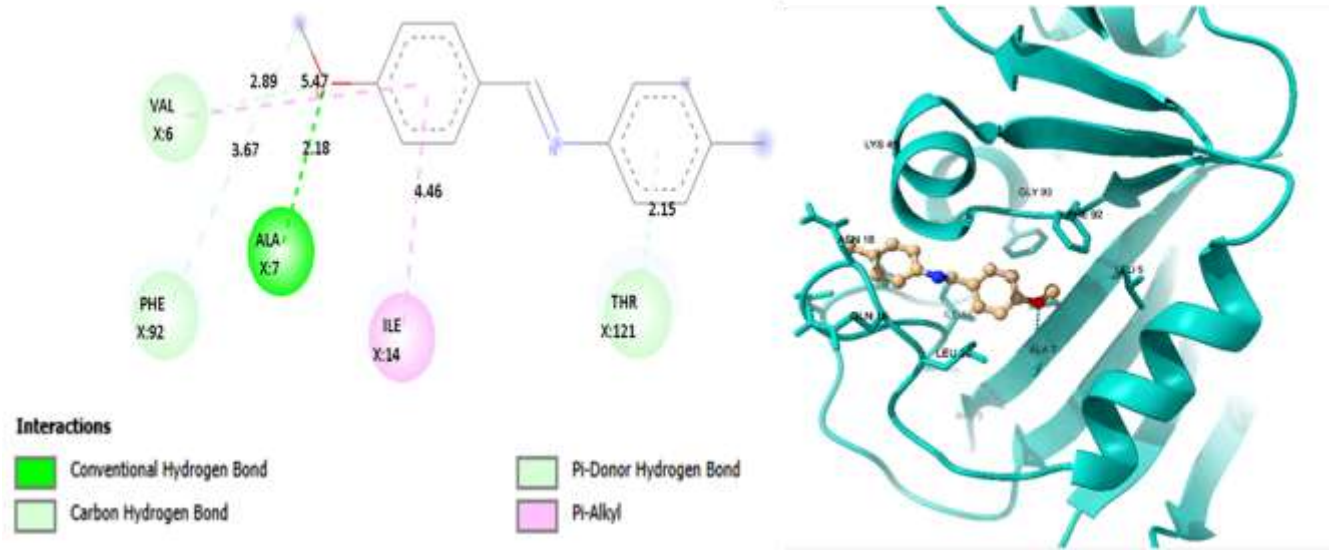

Figure 5: (a) 2D interaction between A2 and 3FYV was illustrated using a Discover Studio diagram showing interaction with one conventional H-bond (green dashed lines) with residues (ALA7), a C-H bond (light green dashed lines) with residues (VAL6, PHE92), and one π-Donor H-bond (lightgreen dashed lines) with residues (THR121) at bond distances (2.18, 2.89,3.67,2.15) Å respectively. Additionally, hydrophobic interactions were observed with ILE14, which contributes to the stabilization of the complex. (b) 3D interaction between A2 and 3FYV was illustrated using ChimeraX, showing that A2 was represented as sticks and balls (O as a red ball, N as a blue ball, and C as a yellow ball) bound with the active pocket of the 3FYV represented as a light sea green ribbon with one H- bond (lightgreen dashed lines) with residue (ALA7).

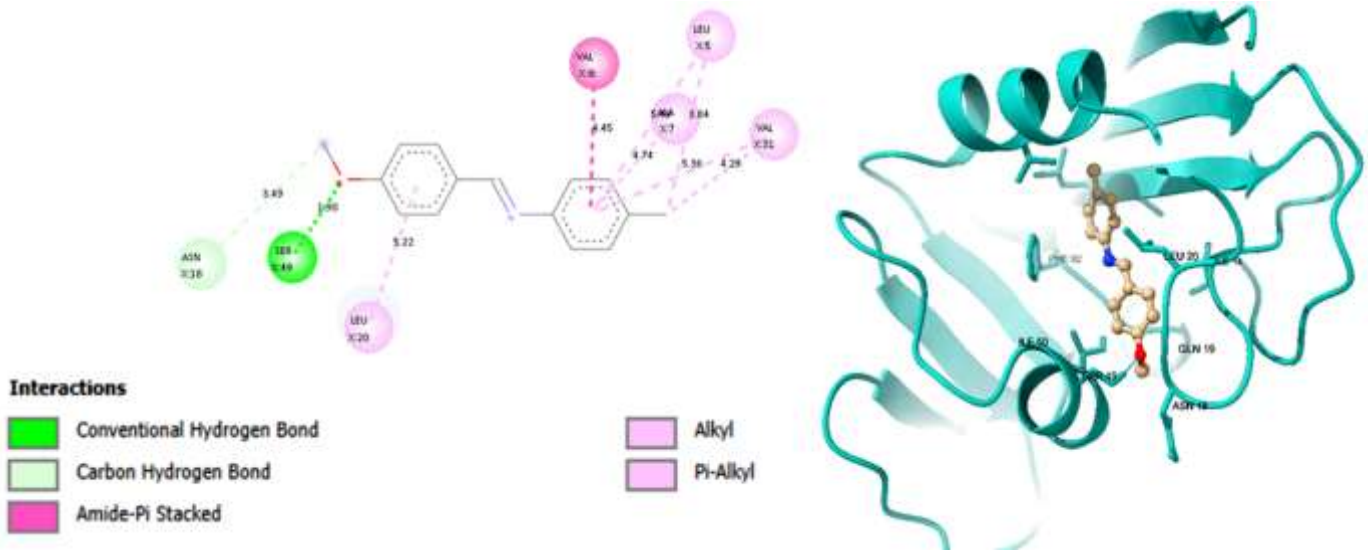

Figure 6: (a) 2D interaction between A3 and 3FYV was illustrated using a Discover Studio diagram showing one conventional H-bond (green dashed lines) with residues (SER49) and one C-H bond (light green dashed lines) with residues (ASN18) at bond distances (1.90, 3.49) Å, respectively. Additionally, hydrophobic interactions were observed with (ALA7, LEU5, VAL31, LEU20, VAL6) which contribute to stabilization of the complex. (b) 3D interaction between A3 and 3FYV was illustrated using ChimeraX, showing that A3 was represented as sticks and balls (O as a red ball). N as a blue ball and C as a yellow ball) bound with the active pocket of the 3FYV represented as a light sea green ribbon with one H-bond (lightgreen dashed lines) with residue (SER49).

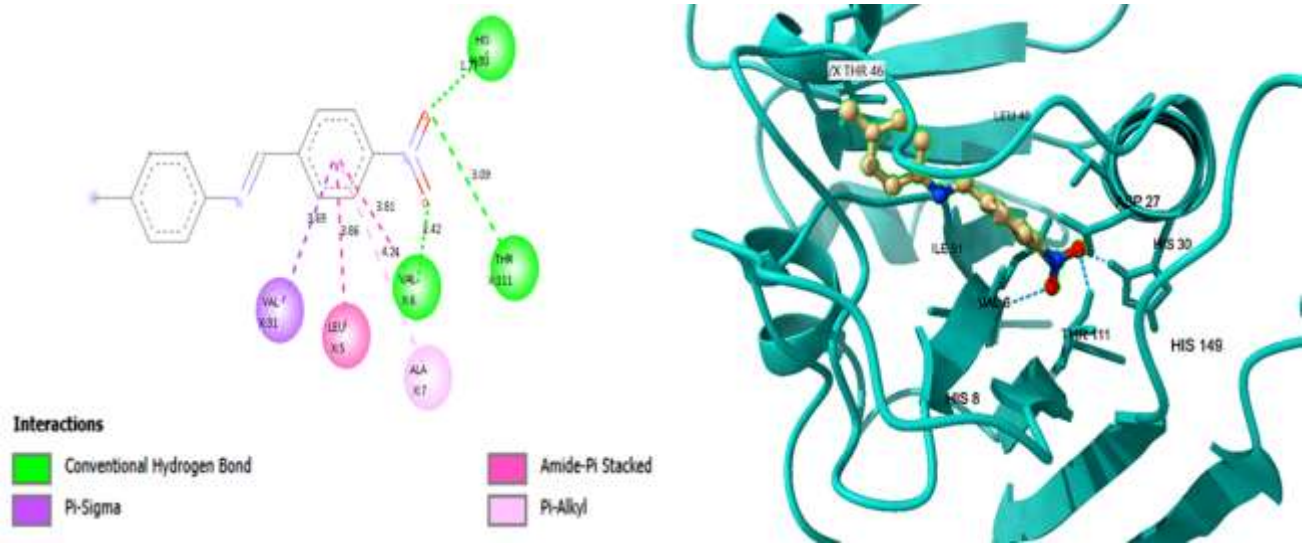

Figure 7: (a) 2D interaction between A4 and 3FYV was illustrated using a Discover Studio diagram showing interaction of 3 H-bonds (green dashed lines) with residues (HIS30, VAL6, THR111) at bond distances (1.77,2.42,3.09) respectively. Additionally, hydrophobic interactions observed were with (ALA7, LEU5, VAL31) which contribute to stabilization of the complex. (b) 3D interaction between A4 and 3FYV was illustrated using ChimeraX, showing the A4 was represented as sticks and balls (O as a red ball, N as a blue ball, and C as a yellow ball) bound with the active pocket of the 3FYV represented as a light sea green ribbon with 3 H-bonds (lightgreen dashed lines) with residues (HIS30, VAL6, THR111).

The visualization with ChimeraX software displayed only one H-bond with residues of HIS30, in contrast to the results from AutoDock 4.2 program and Discover Studio, as illustrated in Figure 4b. In addition, A2 showed one hydrogen bond with ALA7 of the 3FYV enzyme Figure 5(a, b), with bond distance 2.18 Å, Figure 5(a, b). Furthermore, A3 formed one hydrogen bond with ESR49 of the 3FYV, Figure 6(a, b), with bond distance 1.90 Å, Figure 6(a, b). Compound A4 formed three hydrogen bonds with HIS30, THR111and VAL6 of the 3FYV enzyme, with bonds distance 1.77 Å,2.00 Å and 2.47 Å respectively, Figure 7(a,b) [35].

6.7. HYDROPHOBIC INTERACTION

The deformation of the 3FYV with A1 was further facilitated by hydrophobic interaction. The 3FYV-A1 molecule demonstrated four hydrophobic interactions with 3FYV. The hydrophobic contact residues of the 3FYV enzyme were ALA7, LEU5, VAL31, and THR46, as illustrated in Fig. 4a. The residues ALA7, LEU5, VAL31, and THR46 are recognized for their involvement in H-bond formation, which contributes to the stability of the complex binding contact. The binding of the 3FYV-A2 complex comprised a single hydrophobic contact with the amino acid residue ILE14, as depicted in Fig. 5a. The bending of 3FYV with A4 was additionally promoted by hydrophobic contact. The 3FYV A4 compound exhibited three hydrophobic interactions with 3FYV. The hydrophobic contact residues of the 3FYV enzyme were ALA7, LEU5, and VAL31, as illustrated in Fig. 7a. The residues ALA7, LEU5, and VAL31 are recognized for their role in H-bond formation, which contributes to the stabilization of the complex binding interaction. The most stable complex was shown in this study in A1 -3FYV short distance and strong hydrogen bond with HIS30. On the other hand, the least stable interaction was in the A2–3FYV complex, by a longer and weaker hydrogen bond with VAL6. This is because the shorter hydrogen bond distance, the stronger interaction between the enzyme with the prepared compound and the longer hydrogen bond distance, the weaker interaction between enzyme with the prepared compound [36-37].

7. Conclusion

In conclusion, Schiff base compounds A1–A4, with the change of the type of the group substituted on both ends of the –CH=N– group, have been successfully obtained with high yields and confirmed

through spectroscopic analysis. Theoretically, their electronic structures were examined using quantum mechanical methods, including HOMO–LUMO analysis and DFT simulations, to derive *E*gap and other properties. According to the results, compound A2 has a higher aromatic character than the other compounds. The molecular docking research definitively established the connection between the synthesized compounds and the enzyme of *Escherichia coli*. Compound A1 exhibits a high docking score of approximately –7.77 kcal·mol^{-1}, suggesting that Schiff base A1 may have antibacterial properties.

Acknowledgments: The authors express their thanks to staff of the lab of the Department of Chemistry, University of Anbar for their kind support, as well as, to all those who have helped. in the accomplishment of this study.

Conflicts of Interest: According to the authors, a conflict of interest is absent.

Funding: there is no funding received for this work.

References

[1] Da Silva, C. M.; Da Silva, D. L.; Modolo, L. V.; Alves, R. B.; De Resende, M. A.; Martins, C. B.; De Fatima, A.; "Schiff bases: A short review of their antimicrobial activities". *J. Adv. Res.* 2: 1-8, 2011.

[2] Ebead, Y.; Soliman, H.; Abdella, M.; "Experimental and Theoretical Investigation of spectral tautomerism and acid-base properties of Schiff bases derived from some amino acids". *Bull. Korean Chem. Soc.* 31: 850-858, 2010.

[3] Sabry, A.; Farag, R. S.; Abdel-Hady, A. M.; "Synthesis, Characterization and antimicrobial activity of Schiff base (E)-N-(4-(2-hydroxybenzylideneamino)phenylsulfonyl) acetamide metal complexes". *Am. J. Anal. Chem.* 7(3): 233-245, 2016.

[4] Boraei, A. T.; Gomaa, M. S.; El Ashry, E. S.; Duerkop, A.; "Design, selective alkylation and X-ray crystal structure determination of dihydro-indolyl-1,2,4-triazole-3-thione and its 3-benzylsulfanyl analogue as potent anticancer agents". *Eur. J. Med. Chem.* 125: 360-371, 2017.

[5] Wei, L.; Tan, W.; Zhang, J.; Mi, Y.; Dong, F.; Li, Q.; Guo, Z.; "Synthesis, Characterization, and Antifungal activity of Schiff bases of Inulin Bearing Pyridine ring". *Polymers* 7: 371-382, 2019.

[6] Slassi, S.; Fix-Tailler, A.; Larcher, G.; Amine, A.; El-Ghayoury, A.; "Imidazole and Azo-based Schiff bases ligands as Highly active antifungal and antioxidant components". *Heteroat. Chem.* 2019: 1-8, 2019.

[7] Al-Garawi, Z. S.; Tomi, I. H.; Al-Daraji, A. H.; "Synthesis and Characterization of new amino acid-Schiff bases and studies their effects on the activity of ACP, PAP and NPA enzymes (in-vitro)". *J. Chem.* 9(2): 962-969, 2012.

[8] Rhoufal, F.; Guesmi, S.; Ketatni, E.; Jouffret, L.; Obbade, S.; Bahsis, L.; Aflak, N.; et al.; "Nickel(II) and copper(II) coordination complexes based on novel ligands generated in situ from the tetradentate 2,4-pentanedione bis(thiosemicarbazone) and the thiocyanate ion: Network topologies, and computational approaches". *Inorg. Chem. Commun.* 179(2): 114777, 2025.

[9] Abood, H. S.; Ramadhan, U. H.; Hamza, H.; "Synthesis and anti-inflammatory activity study of Schiff bases complexes". *Biochem. Cell. Arch.* 20(2): 5627-5631, 2020.

[10] Abdullah, H. I.; Al-Joboury, W. M.; Aljoboury, I. F.; Hameed, I. K.; Al-Badrany, K. A.; Abdulqader, M. A.; "Synthesis and Characterization of Schiff base Compounds Produced from 6-Bromo-4-Fluoro-2 Aminobenzothazol Assessment against Antibacterial Activity". *AUIQ Complement. Biol. Syst.* 2(1): 118-130, 2025.

[11] Choudhary, M. I.; Abbas, G.; Ali, S.; Shuja, S.; Khalid, N.; Khan, K. M.; Rahman, A.; Basha, F.; "Substituted benzenediol Schiff bases as promising new anti-glycation agents". *J. Enzyme Inhib. Med. Chem.* 26(1): 98-103, 2011.

[12] Patel, R. N.; Patel, P. V.; Desai, K. R.; Purohit, P.; Nimavat, K.; Vyas, K.; "Synthesis of new heterocyclic Schiff base; Thiazolidinone; Azetidinone compounds and their antibacterial activity, and anti-HIV activities". *Heterocycl. Lett.* 2(1): 99-105, 2012.

[13] Meeran, S.; Tajndeen, S. S.; Dusthakeer, A.; Shabeer, T. K.; "An Insight into the Anti-tubercular potential of Schiff bases". *J. Pharm. Chem. Biol. Sci.* 6(3): 158-177, 2018.

[14] Bhat, M. A.; Al-Omar, M. A.; "Synthesis, Characterization and in vivo anticonvulsant and Neurotoxicity sereening of Schiff bases of phthalimide". *Acta Pol. Pharm.* 68(3): 375-380, 2011.

[15] Saranya, M.; Ayyappan, S.; Nithya, R.; Sangeetha, R. K.; Gokila, A.; "Molecular structure, nbo and homo-lumo analysis of quercetin on single layer graphene by density functional theory". *Dig. J. Nanomater. Biostruct.* 13(1): 97-105, 2018.

[16] Osman, I. O.; "DFT Study of the structure, reactivity, natural bond orbital and hyperpolarizability of thiazole azo dyes". *Int. J. Mol. Sci.* 18: 239, 2017.
[17] Salama, M. M.; Ahmed, S. G.; Hassan, S.; "Synthesis, Characterizations, Biological, and Molecular Docking studies of some amino acid Schiff bases with their Cobalt(II) complexes". *Adv. Biol. Chem.* 7: 182-194, 2017.
[18] Rajaraman, D.; Sundararajan, G.; Loganath, N. K.; Krishnasamy, K.; "Synthesis, molecular structure, DFT studies and antimicrobial activities of some novel 3-(1-(3,4 dimethoxyphenethyl) -4,5-diphenyl-1H-imidazol-2-yl)-1H-indole derivatives and its molecular docking studies". *J. Mol. Struct.* 1127: 597-610, 2017.
[19] Neese, F.; Wennmohs, F.; Becker, U.; Riplinger, C.; "The ORCA Quantum Chemistry Program Package". *J. Chem. Phys.* 152(22): 224108, 2020.
[20] Orio, M.; Pantazis, D. A.; Neese, F.; "Density functional theory". *Photosynth. Res.* 102: 443-453, 2009.
[21] Weigend, F.; "Accurate Coulomb-Fitting Basis Sets for H to Rn". *Phys. Chem. Chem. Phys.* 8(9): 1057-1065, 2006.
[22] Thakor, P. M.; Patel, J. D.; Patel, R. J.; Chaki, S. H.; Khimani, A. J.; Vaidya, Y. H.; Chauhan, A. P.; et al.; "Exploring New Schiff Bases: Synthesis; Characterization; and Multifaceted Analysis for Biomedical Applications". *ACS Omega* 9(33): 35431-35448, 2024.
[23] Rajkumar, P.; Selvaraj, S.; Anthoniammal, P.; Kumar, A. R.; Kasthuri, K.; Kumaresan, S.; "Structural (monomer and dimer); spectroscopic (FT-IR; FT-Raman; UV–Vis and NMR) and solvent effect (polar and nonpolar) studies of 2-methoxy-4-vinyl phenol". *Chem. Phys.* 7(4): 100257, 2023.
[24] Mukhlif, M. G.; Mahdi, O. J.; Bichan, M. J.; "Synthesis; characterization; molecular docking; and computational study of novel spirothiazolidinone compounds". *J. Mol. Struct.* 1330: 141517, 2025.
[25] Bichan, M. J.; Al-Bayati, Y. K.; AL-Abady, F. M.; Awwadi, F. F.; "Theoretical study of molecularly imprinted polymers prepared for homatropine methylbromide". *J. Polym. Res.* 30: 142, 2023.
[26] Shearer, G. C.; Chavan, S. M.; Bordiga, S.; Svelle, S.; Olsbye, U.; Lillerud, K. P.; "Defect Engineering: Tuning the Porosity and Composition of the Metal-Organic Framework UiO-66". *Chem. Mater.* 28(11): 3749-3761, 2016.
[27] Mulliken, R. S.; "Criteria for the Construction of Good Self-Consistent-Field Molecular Orbital Wave Functions; and the Significance of LCAO-MO Population Analysis". *J. Chem. Phys.* 36: 3439-3438, 1962.
[28] Rigby, J.; Izgorodina, E. I.; "Assessment of atomic partial charge schemes for polarisation and charge transfer effects in ionic liquids". *Phys. Chem. Chem. Phys.* 15: 1632, 2013.
[29] Berg, J. M.; Tymoczko, J. L.; Stryer, L.; "*Biochemistry*". 9 ed.; W. H. Freeman and Company and Sumanas, Inc.: New York, 2002.
[30] Pinzi, L.; Rastelli, G.; "Molecular docking: Shifting paradigms in drug discovery". *Int. J. Mol. Sci.* 20(18): 4331, 2019.
[31] Abd El-Lateef, H. M.; Ali, A. M.; Khalaf, M. M.; Abdou, A.; "New Fe(III); Co(II); Ni(II); Cu(II); and Zn(II) mixed-ligand complexes :structural; DFT; biological; and molecular docking studies". *Bull. Chem. Soc. Ethiop.* 38(2): 397-416, 2024.
[32] Bhatia, A.; Singh, B.; Arora, R.; Arora, S.; "In vitro evaluation of the α-glucosidase inhibitory potential of methanolic extracts of traditionally used antidiabetic plants". *BMC Complement. Altern. Med.* 19(1): 74, 2019.
[33] Sadiq, A.; Rashid, U.; Ahmad, S.; Zahoor, M.; AlAjmi, M. F.; Ullah, R.; Noman, O. M.; et al.; "Treating Hyperglycemia From Eryngium caeruleum M. Bieb: In-vitro α-Glucosidase; Antioxidant; in-vivo Antidiabetic and MolecularDocking-Based Approaches". *Front. Chem.* 8: 558641, 2020.
[34] Pinzi, L.; Rastelli, G.; "Molecular docking: Shifting paradigms in drug discovery". *Int. J. Mol. Sci.* 20(18): 4331, 2019.
[35] Salmaso, V.; Moro, S.; "Bridging molecular docking to molecular dynamics in exploring ligand-protein recognition process: An overview". *Front. Pharmacol.* 9(923), 2018.
[36] Gurung, A. B.; Ali, M. A.; Lee, J.; Farah, M. A.; Al-Anazi, K. M.; "An updated review of computer-aided drug design and its application to COVID-19". *Biomed. Res. Int.* 2021(1): 8853056, 2021.
[37] Muhammed, M. T.; Aki-Yalcin, E.; "Homology modeling in drug discovery: Overview; current applications; and future perspectives". *Chem. Biol. Drug Des.* 93(1): 12-20, 2019.guides.lib.berkeley+1